Electron-Pion Discrimination with a Scintillating Fiber Calorimeter

D. Acosta[1], S. Buontempo[2], L. Calôba[3], M. Caria[4], R. DeSalvo[5a], A. Ereditato[2],

R. Ferrari[6], M. Fraternali[7], G. Fumagalli[6], V.G. Goggi[5,6], F. G. Hartjes[8], W. Hao[5b†],

Th. H. Henkes[9], A. Henriques[5a,10], L. Linssen[5a], M. Livan[4], A. Maio[10], L. Mapelli[5],

K. H. Meier[5‡], R.M. Mondardini[13], B. Ong[1], H. P. Paar[1], F. Pastore[6], M. Pereira[10],

L. Poggioli[11], G. Polesello[5], C. V. Scheel[5a,8], J. M. Seixas[3,5b], A. Simon[12], M. Sivertz[1],

P. Sonderegger[5], M. N. Souza[3], Z. D. Thome[3], V. Vercesi[5], Y. Wang[5b†], R. Wigmans[5a,8], C. Xu[5b†]

1) University of California, San Diego, USA; 2) Universita di Napoli and INFN Sez. Napoli, Italy;

3) COPPE/EE/UFRJ, Rio de Janeiro, Brazil; 4) Universita di Cagliari and INFN Sez. Cagliari, Italy;

5) CERN, Geneva, Switzerland; 5a) CERN (LAA project), Geneva, Switzerland;

5b) CERN (World Lab Fellowship), Geneva, Switzerland; 6) Universita di Pavia and INFN Sez. Pavia, Italy;

7) Universita di Palermo and INFN Sez. Pavia, Italy; 8) NIKHEF-H, Amsterdam, The Netherlands;

9) Max Planck Institut, Heidelberg, Germany; 10) LIP, Lisbon, Portugal;

11) LPNHE, Université Paris VI & VII, Paris, France; 12) Universität Heidelberg, Germany;

13) Cornell University, Ithaca, USA

ABSTRACT

We report on an experimental study of a variety of techniques for discriminating between (isolated) electrons and pions in a lead and scintillating fiber calorimeter without longitudinal segmentation. Using information from the lateral shower development, from a pre-shower detector, from the time structure of the signals, or from a combination of these we measure pion rejection factors of up to several thousand while maintaining electron efficiencies of 95% or higher.

---

† On leave from IHEP, Bejing, China.
‡ Now at DESY, Hamburg, Germany.

1. Introduction

The scintillating fiber calorimeter technique has been developed for use at future high energy hadron colliders. Some of its notable properties are: speed of response, compensation, linearity, good energy resolution for electromagnetic and hadronic showers, uniformity of response as a function of impact point and angle, hermeticity, ease of lateral segmentation, spatial resolution, low noise, and sensitivity to minimum ionizing particles.

We report on the electron-pion discrimination[1] properties of a scintillating fiber calorimeter for the case of isolated electrons. The work described in this paper has been carried out in the framework of the CERN-LAA project. Although most of the analysis in this paper is concerned with offline methods, an important goal was to find techniques suitable for fast triggering. Further studies aim to implement these ideas at the trigger level and to find methods to recognize electrons in or near a jet.

Electron-pion discrimination can be achieved with a calorimeter by exploiting the very different longitudinal and lateral energy deposit profiles of electromagnetic and hadronic showers. While having excellent lateral segmentation capability (without compromising the properties listed above), the fiber calorimeter does not lend itself easily to longitudinal segmentation. Longitudinal segmentation is often thought to be essential in order to obtain sufficient electron-hadron discrimination. Lateral and longitudinal energy deposit profiles of showers are correlated but longitudinal segmentation has an advantage over lateral segmentation in two processes that may lead to pion-electron confusion:

   a. Charge exchange where the charged pion produces a single neutral pion with the same energy, leading to an electromagnetic shower that develops deeper into the calorimeter because its starting point is on average deeper into the calorimeter.

   b. Hadronic shower development with predominantly neutral pion production in the first generation, leading to essentially electromagnetic shower development at greater depth.

Instead of longitudinal segmentation, the SPACAL design uses one or more of the following techniques:

   a. Lateral shower development: typical hadron showers spread over a larger area than electromagnetic showers.

   b. Longitudinal shower development: a thin pre-shower detector in front of the calorimeter samples the starting point of showers.

c. Time structure: the time structure of the calorimeter signal is very different for electrons and pions[2,3] . It can be used as an indication of the longitudinal shower development.

We have investigated the electron-pion discrimination capabilities of a prototype scintillating fiber calorimeter with modest lateral segmentation, no longitudinal segmentation, and with a pre-shower detector in front. We find that, for energies of 40 GeV or larger, pion rejection factors of several hundred to one thousand can be obtained from the lateral shower energy distribution or the timing information respectively. Pion rejection factors of several thousand are found when both the lateral shower distribution and the pre-shower detector are used.

2. Calorimeter

A prototype compensating calorimeter, consisting of 20 towers, was constructed in preparation for the construction of a larger calorimeter with 155 towers. It has parallel (as opposed to projective) geometry and consists of scintillating fibers of 1 mm diameter, embedded in a lead matrix in an hexagonal pattern. The lead and fiber is in the volume ratio of 4:1. The fibers used were SCSF-38 from Kyowa[4] . The fiber spacing is 2.21 mm center to center. The front faces of the fibers were mirrored (85% reflectivity) by aluminum sputtering. This nearly doubles the effective attenuation length of the fibers to about 8 m and thereby flattens the response to hadron showers produced at different depths. The lead matrix is formed by stacking 1.91 mm thick, 48.6 mm wide, and 2 m long grooved lead strips with fibers in the grooves.

The fibers have been grouped to form 20 towers, arranged and numbered as shown in Fig. 1. Each tower has an hexagonal cross section (86 mm apex-to-apex) and is 2.00 m long. The fibers within each tower were taken from batches of fibers that have similar optical characteristics in terms of attenuation length and light yield, based upon measurements done on 5% of the fibers in each batch. The nuclear interaction length[5] (λ_I) of the fiber and lead combination is 21 cm; thus the calorimeter is deep enough, but not wide enough, to contain hadronic showers. The fibers of each tower are coupled to an hexagonal lightpipe, 42 mm apex-to-apex and 79 mm long, which in turn is coupled to a custom specification 8 stage (7 dynodes) photomultiplier (Philips XP2282). The photomultiplier base is cooled by a flow of air for gain stability. The photomultiplier signals were fed into an active splitter, one output of which gave a gain 1 signal. The other signal was amplified by a factor of approximately 10-12. Both signals were digitized with a LeCroy 2280 series charge-sensitive ADC system with a gate width of 400 ns. The 12 bit ADC's gain was 4 counts per pC (for a 1000 pC full scale).

Sparse data readout was enabled: a digitizer output had to be four or more counts over pedestal in order to be written to tape. The high voltages of the photomultipliers of the 20 towers were set to get approximately 4 pC per GeV at the photomultiplier output. Thus in the low gain signal path we have about 60 MeV per ADC channel and in the high gain path about 6 MeV per ADC channel. Thus the readout threshold corresponds to a cut at 25 MeV in the high gain channels. At the beginning of each run a precise calibration of the cable and the ADC's of each calorimeter module was performed by injecting a known amount of charge by means of an electronic pulser under computer control.

3. Beam

The beam tests reported here were done with the H2 beam of the Super Proton Synchrotron at CERN in December 1989 and in April 1990. The layout of the trigger counter telescope and its position relative to the prototype calorimeter are shown schematically in Fig. 2. BC1 and BC2 are beam chambers, each with x and y readout. S_1, S_2, and S_3 are trigger counters with dimensions $10 \times 10 \, \text{cm}^2$, $15 \times 15 \, \text{cm}^2$, and $3 \times 3 \, \text{cm}^2$ diameter respectively. S_4 and S_5 are beam defining counters with dimensions of $0.5 \times 0.5 \, \text{cm}^2$. S_6 is a $15 \times 15 \, \text{cm}^2$ by 1 cm thick scintillation counter just behind a 5.3 mm ($1.5 \, L_{\text{rad}}$, $0.055 \lambda_I$) plate of tungsten and a 2.8 mm ($0.5 \, L_{\text{rad}}$, $0.016 \lambda_I$) plate of lead. All together S_6 forms the pre-shower detector.

Data for electron-pion discrimination studies were taken with negative pions and electrons at 40, 80, and 150 GeV, entering the calorimeter at different impact points, among them points A and B, indicated in Fig. 1. During the April 1990 beam tests the beamline had a 10 m long airgap and streamer chamber frames about 50 m upstream of the calorimeter. This corresponds to about 3 % of a radiation length. Its effects include a radiative tail in the electron energy spectrum as observed in the calorimeter. Such tails were absent in the December 1989 data. Part of the pion data were taken with a 25 mm thick lead sheet in the beam, placed about 80 m upstream, to remove the small residual electron contamination in the pion beam.

The beams were incident at 3 degrees with respect to the fiber direction. For the timing studies the trigger consisted of a coincidence between S_1, S_2, S_3, S_4, and S_5. For the lateral shower profile and the pre-shower studies, the electron trigger consisted of a coincidence between S_1, S_2, and S_3 while the pion trigger consisted of a coincidence between S_1, S_2, S_3, and S_6 with the discriminator threshold of S_6 set at approximately 1.5 minimum ionizing pulse height (minI). This threshold was below the offline cut on the pre-shower detector pulse height

(see below) but high enough to reduce the pion trigger rate by about a factor 10. This reduction was important to obtain enough statistics as the final pion rejection factor was several thousand. At each energy a pion run was taken without S_6 in the trigger for normalization of the runs taken with S_6 in the trigger. Beam rates into the calorimeter were on the order of 10^3 particles per 2.6 sec long spill. The repetition time of the SPS was 14.4 sec. The readout rate was about 100 events per spill, except for the time structure studies where about 3 events per spill were readout from the digitizing oscilloscope.

The pion beam had very little electron contamination. Estimates of the electron contamination in the pion beam were made by comparing the pion misidentification probability for runs with and without a 25 mm thick lead filter placed in the beam upstream of the last bending magnets. The electron contamination in the pion beam was seen to vary from 1:500 at 40 GeV to 1:1700 at 150 GeV. With the lead filter the electron contamination was measured to be less than $1{:}10^5$ at 40 GeV.

Offline event selection required a single track by a cut on the pulse height of S_1, S_2, and S_3 between 0.5 and 1.7 minI. The values for the coordinates x and y measured in each of the BC1 and BC2 beam chambers had to agree within 1 cm. Events from beam halo particles were removed by applying cuts on the beam spot by means of cuts on x and y.

4. e - π Discrimination from Lateral Shower Development

A central idea underlying electron-pion discrimination in the scintillating fiber calorimeter is the fact that hadronic showers typically have larger lateral dimensions than electromagnetic showers. We report on two simple methods to characterize these shapes. The first method (Sec. 4.1) involves counting the number of towers over an energy threshold that participate in a shower. The second method (Sec. 4.2) uses a more quantitative estimate of the lateral energy spread and cuts on the fraction of shower energy outside a small core.

4.1 Counting Towers over Threshold

In this method we count the number of towers with energy over a given energy threshold, E_{thr}. In Fig. 3 we plot, separately for electrons and pions, the number of events as function of the number of towers that each have an energy exceeding $E_{\mathrm{thr}} = 0.4\,\mathrm{GeV}$. The data are for 80 GeV particles incident at point A, the center of the central tower, see Fig. 1. For the electron sample an energy cut around the electron peak was made to reduce the pion background. As expected,

the number of towers that contribute to an electron shower is smaller than the number that contribute to a hadron shower. There are two enhancements in the electron curve. The lower one is from electrons. The upper one is due to pion contamination in the electron sample that remain after the energy cut, as can be seen from a comparison with the pion curve. As an example of the use of this method, define electrons as particles that have seven or fewer towers. The electron efficiency for this cut is 98.8% while 1.0 % of the pions pass this same cut. Thus we have a pion rejection factor of 100 by a simple counting algorithm. This procedure has been repeated for other impact points, other particle energies, and other threshold energies. We have also repeated the procedure using a cut at three towers instead of at seven. Similar results are obtained, but they are much more sensitive to the position of the impact point and so this was not considered useful for triggering. Energy dependent thresholds were chosen to keep the electron efficiencies near 98 %. The resulting pion fractions passing the electron selection cuts and the electron efficiencies obtained for the seven-tower cut are listed in Table 1.

The energy thresholds needed to retain high electron efficiency are observed to increase less than linearly with the energy of the incident particle. The fraction of pions passing the electron cuts decreases with increasing energy. If the same E_{thr} cuts for 7 towers for the central impact point A are used with data taken at the corner point B, the electron efficiencies are virtually unchanged, while the fraction of pions passing increases slightly. The numbers for the pions listed in Table 1 are slightly overestimated (the rejection factor is underestimated). This is because April 1990 data was used for this analysis and there was about 3% of a radiation length of material 50 m upsteam of the calorimeter. The accompanying bremsstrahlung photon tends to increase the lateral spread of the electromagnetic shower which will reduce the electron efficiency and force a higher threshold cut. This in turn will increase the fraction of pions which pass the electron selection cuts.

4.2 LATERAL DISTRIBUTION OF ENERGY DEPOSIT

In the calculation of electromagnetic shower energy a summation over at least three towers must be performed unless one uses knowledge of the particle's impact point. For hadronic showers the summation must be over a much larger number of towers. The lateral distribution of energy deposits can be more precisely characterized by introducing a quantity called the containment C defined as

$$C = \frac{\sum_{i \in \{3\}} E_i}{\sum_{i \in \{12\}} E_i} \tag{1}$$

The cluster {3} of three towers is defined as the three neighboring towers with the largest energy sum. The cluster of three is surrounded by nine neighbouring towers (see Fig. 1). $\sum_{i \in \{12\}} E_i$ is the sum of the energies of these nine towers plus the three core towers. No use of the known impact point or beam energy was made so as to simulate a possible (low level) trigger strategy. In Fig. 4 the containment C is plotted for 80 GeV electrons and pions incident near point A. Note the difference in horizontal scale. It is seen that the values of C for electrons and pions differ greatly. A cut $C \geq 0.970$ gives a pion rejection factor of 150 and is about 98 % efficient for electrons at 80 GeV.

The analysis has been repeated for other impact points and energies using the same cut on C. The resulting pion fraction passing electron selection cuts and the corresponding electron efficiencies are given in Table 2. We have measured that the electron-pion discrimination improves when the impact point is near the boundary of several towers. This is because the containment for electrons is seen to be better (C is higher) in that case allowing one to raise the cut on C for a given electron efficiency (this was not done for Table 2 so as to maintain simplicity for trigger strategies). The containment for pions is essentially independent of impact point so that a higher cut on C rejects a larger fraction of pions. For the same reason one might also expect to obtain better electron-pion discrimination if the towers had the smaller cross section presently foreseen for collider detectors. The containment is a strong function of the pion energy, and obvious improvements in the algorithm can be made. For example one can make the cut on C a function of the measured energy or dependent upon the energy sharing among the towers in the cluster {3}.

With a cut on C specified in three decimal places, one might think that the calibration constants of each tower must be precisely known for the cut to work properly. We show however that this is not needed for this purpose. The pions in the confusion region have $C \geq 0.970$. This means that in (1) the numerator and denominator are almost equal (and that the lateral size of the pion shower is small). As a consequence variations in the numerator and denominator of (1) due to incorrect calibration constants are correlated, leaving the numerical value of C essentially unchanged. To test this assumption, the energies of each tower were multiplied by a random number taken from a Gaussian distribution (different ones for each event) with a mean of 1.0 and a standard deviation of 0.1. This simulates the situation where a detector's calibration is off by 10 % and each event deposits its energy in a different region of the detector. The above analysis was repeated. The resulting pion rejection factor was unchanged while the electron efficiency dropped by 0.5 %.

Electron-pion discrimination studies were done[6] with the testbeam data on

image processors using the ratio of the cluster {3} to the surrounding nine towers. Studies are underway to investigate the possibility of using these commercially available image processors in triggering.

5. e - π Discrimination from Pre-Shower Detector

The pre-shower detector pulse height is plotted in Fig. 5 for 80 GeV pions and electrons. The abscissa is in units of minI pulse height. Most pions give one minI unit of pulse height while the electron's pulse height distribution peaks at 4.5 minI. For a given cut on the pre-shower pulse height one finds a pion rejection factor and a corresponding electron efficiency. For example a cut at 1.75 minI gives a pion rejection factor of 13.5 and maintains an electron efficiency of 98%. The 7.4% of the pions passing the preshower cut are due to inelastic interactions in the pre-radiator and to the tail of the Landau distribution of the pulseheight for minimum ionizing particles. The contribution from inelastic interactions is calculated to be 5.8%, using the dimensions of the pre-shower detector materials given in Sec. 3 and including the 5 mm scintillator material in the S_4 and S_5 counters and the air downstream of S_2 (interactions there are not rejected by the minimum ionizing pulseheight requirments in S_1, S_2, and S_3). The pre-shower detector was not optimized for good resolution. Better readout with for example a silicon detector is expected to give still better pion rejection.

The analysis has been repeated at other energies. The results are given in Table 3. The pre-shower cut is chosen to be independent of energy. The resulting electron efficiency has therefore a slight energy dependence. It is seen that the pion rejection factor is in all cases larger than 10.

6. e - π Discrimination from Lateral Shower Development and Pre-Shower Detector

Still better electron-pion discrimination can be obtained when several of the cuts discussed above are applied simultaneously. Of special interest in this are the correlations that exist between different cuts. We define a correlation r as

$$r = \ln \frac{f_{12}}{f_1 f_2} \tag{2}$$

where f_i is the fraction of events that pass the cut i (when acting on the same event sample) and f_{12} is the fraction of events that pass both cuts 1 and 2. There is an obvious extension of the formula to more than two cuts. When $r \neq 0$ the cuts are correlated. Interestingly, we find $r < 0$ for the combination

8

of a pre-shower cut and a lateral shower development cut. This means that the effects of the combined cuts exceed what one might expect from each cut separately. The effect is caused by the larger lateral spread of hadronic showers when their starting point is in the pre-shower detector, about 10 cm in front of the calorimeter. This is confirmed by the fact that such showers exhibit a larger leakage out the sides of the calorimeter. These showers have therefore an enhanced probability to be recognized as hadronic showers from their lateral size.

The pion rejection factor obtained with the combined cuts was determined from special runs where a 25 mm thick lead filter was put into the beam about 80 m upstream of the calorimeter to remove the small electron contamination in the pion beam. We have tested the effectiveness of this lead filter by putting it in a 40 GeV electron beam. We found that about 5 in 1000 electrons incident on the filter triggered the S_1, S_2, S_3 coincidence. This implies that (at 40 GeV) less then 0.5 % of the electron contamination remains in the pion beam. By comparing the pion runs with and without the lead filter it is possible to estimate the electron contamination. This was typically 1:500 at 40 GeV dropping to 1:1700 at 150 GeV when there was no lead filter in the beam. Thus the electron contamination in the pion beam with the lead filter in the beam is less then $1:10^5$ and therefore has a negligible effect on the measured pion rejection factor.

In Table 4 we give the fraction of pions passing electron selection cuts, the correlation factor (as defined in (2)), and the electron efficiency, obtained with a combination of cuts on the containment and the pre-shower detector pulseheight as described in Sec. 4 and 5 respectively. The fraction of pions passing electron selection cuts and the corresponding electron efficiency are plotted in Fig. 6 as function of the containment (with a preshower pulseheight cut at 1.75 minI), and in Fig. 7 as function of energy. It is seen that pion rejection factors of 1500 − 2400 are obtained for pion energies in the range 40 to 150 GeV while maintaining excellent electron efficiency. Also indicated in Table 4 and Fig. 7 are the estimated contributions from charge exchange, as discussed in Sec. 1. This contribution is estimated by calculating[7] the probability for charge exchange followed by pair-production by at least one of the two photons upstream of the calorimeter. It is seen that the pion rejection factor is a factor 30 − 100 from the limits imposed by the charge exchange cross-section.

7. e - π Discrimination from Time Structure

Data taken with a digitizing oscilloscope have shown that the analog signals coming from the calorimeter are not only fast but also that some characteristics of their pulse shape can be used for discriminating between electrons and pions[2,3]. The electron signals show pulse shapes characteristic of scintillators (Fig. 8a), whereas pion pulses display a more complex structure (Fig. 8b, c, d, e) reflecting the longitudinal development of hadronic showers.

The most significant differences between electron and pion signals come from the differences in the shower starting point and in the longitudinal shower development. Hadronic showers result in broader signals (Fig. 8b, c, d, e) and even signals with a separate second maximum (Fig. 8c, d) for the cases in which the direct light and the light reflected off the front end of the aluminized scintillating fibers are sufficiently well separated in time. Another, but less easily detectable difference between electron and pion signals are the slight differences in the tails of the signals due to the neutron component in hadronic showers.

Two methods that use the signal time structure for electron-pion discrimination have been investigated. The first method (Sec. 7.1) exploits signal differences by looking at the width of the calorimeter signals. The second method (Sec. 7.2) employs electronic filtering techniques to remove elements of the signals that are common to electrons and pions.

7.1 PULSE WIDTH TECHNIQUE

In this section we describe a method to provide a first level trigger signal from the calorimeter alone for the identification of (isolated) electrons. Such a trigger signal is required to be independent of the impact point and independent of the energy of the particles. The $\Sigma 7$-FWFM method presented below fulfills these minimum requirements.

The signal from each calorimeter tower is summed with its six neighbouring towers, see Fig. 1. The seven signals are timed relative to each other with a precision of 0.5 ns. As electron showers are already well contained in a cluster of three neighboring towers (see Sec. 4.2), the resulting $\Sigma 7$-signal for electrons is independent of the impact point on the central tower. Hadronic showers are only contained to about 80 % in seven towers and the variation in pulse height due to different impact points on the central tower are negligible with respect to the large fluctuations due to the leakage. Moreover, as will be seen later, their pulse heights are irrelevant because only their change in shape with respect to the 'standard' electron pulse shapes are of importance. If the signal shapes scale with the energy, then the width at a given fraction of the pulse amplitude

can discriminate between electrons and pions in an energy-independent way. An appropriate fraction was found to be one-fifth and the corresponding width is called FWFM: Full Width at one Fifth Maximum. This is a compromise between a lowest possible value necessary for best electron-pion discrimination and a highest possible level which would yield the smallest possible width and thereby the smallest possible deadtime for triggering.

The output of the active summing circuit is fed into a LATE-CFD (Leading And Trailing Edge - Constant Fraction Discriminator) set at 20 % of the pulse amplitude. The circuit triggers on both signal slopes and provides a logic signal (and its complement) with a length identical to the FWFM of the input signal. The LATE-CFD was designed in such a way that the only adjustable parameter is the fraction of the amplitude. The leading edge of the FWFM signal is available 25 ns after the arrival of the analog input signal at the input of the summing circuit. The circuit has a deadtime of 85 ns which is due to this internal delay and the total length of the analog calorimeter pulses. For triggering purposes, the LATE-CFD can be followed for example by a Time-to-Amplitude-Converter on which one can set an amplitude threshold for discriminating between the electron and pion FWFM-distributions. During our beam tests, we checked the performance of the circuit by monitoring the measured FWFM signals. For this purpose, the leading edge of the logic signal and the trailing edge of the complementary signal were discriminated and sent to 2 TDC inputs started by the common trigger signal. The time difference between the TDC channels then measures the width of the signal.

Distributions of the FWFM for 80 GeV electrons and pions are shown in Fig. 9. Data from impact points A and B are plotted together. Electron contamination in the pion beam was reduced by requiring the pre-shower pulse height to be less than 1.5 minI. The pion fraction passing electron selection cuts and the corresponding electron efficiency are shown in Fig. 10 as a function of the FWFM threshold for the 80 GeV data. We find a pion rejection factor of 800 for an electron efficiency of better than 99%. The peak position and the standard deviation (0.20 ns) of the electron distributions are unchanged within the error for different energies and different impact points. The same is true for the much broader pion FWFM-distributions. Therefore the position of the minimum between the well-separated electron and pion distributions is energy-independent and a fixed cut can be made to separate the two distributions. The fractions of pions passing electron selection cuts and the corresponding electron efficiencies are given in Table 5 for different energies and for a common threshold.

The pion beam used for these studies had an electron contamination at a level which was not negligible compared to the electron-pion discrimination that can be

achieved with the Σ7-FWFM method. Therefore the preshower counter was used in this analysis to remove the electron contamination and it could therefore not be used to study the electron-pion discrimination from combined time structure and pre-shower cuts. The requirement of a preshower pulseheight of less than 1.5 minI provides a pion sample pure to $1:10^4$. The only effect of this cut is to select a pure pion beam of single non-showering pions entering the calorimeter. The resulting electron-pion discrimination is due to the Σ7-FWFM method alone.

7.2 ANALOGUE FILTERING TECHNIQUE

Another approach to using the intrinsic differences between the time structure of electromagnetic and hadronic shower signals is to design a filter that is matched to the signal shape characteristic for electromagnetic showers. Since we want to trigger on electrons which have very stable pulse forms, such a filter might be a fast, cheap, and efficient solution.

Before being able to design a matching filter, one should know the pulse shape to be matched in as great detail as possible. Also, it is important to know the individual contributions of all the different sources affecting the shape of the detected signal. Apart from the intrinsic factors related to the physics of the shower development and to the production and the transport of the scintillation light, the detected pulse shapes are also affected by contributions from cables and possibly other RC components, and from the device used for converting scintillation light into electron signals (the photomultiplier in this case). It is important to unfold these instrumental effects because:

a. One wants the matching filter to be independent of these effects in order to avoid redesigning it every time the setup is changed.

b. By eliminating the instrumental effects which are common to both the electromagnetic and hadronic signals one may hope to be able to better discriminate between these.

The instrumental effects were measured and compensated for. The effect of the fast signal cable (type C-50-6-1) was measured by studying the response to a fast (rise time 70 psec) step function. By using a linear combination of three exponential functions to describe the resulting impulse response, the cable's transfer function could be accurately compensated for. The contribution of the photomultiplier was determined and also compensated for by studying the single-photoelectron response. Its impulse response can be approximated by a double pole circuit. More details are available in Ref. 8. Knowing the details of these instrumental effects, they were unfolded using a preprocessing filter, which was designed and built specially for this purpose. To study the performance of this

filter, shower signals were recorded with a fast (1 Gsample/sec) digital storage oscilloscope. The signals were obtained by summing the pulses from a cluster of seven modules (compare Sec. 7.1). Both the filtered and the unfiltered signals were recorded for each event. Data were taken at 40, 80, and 150 GeV and at the impact points A and B (see Fig. 1).

Analysis of the digitized oscilloscope data showed that the electron-pion discrimination clearly improves as a consequence of the filtering. Because of the low trigger rate and because of the excellent electron-pion discrimination, the number of recorded pion events passing electron selection cuts was very small. Therefore it was not possible to determine whether the improvement in pion rejection obtained by removing the instrumental effects depends upon the energy or impact point. Taking all data together it is found that an electron selection cut on the FWFM of the filtered signals reduced the number of pions by 30% relative to making electron selection cuts on the unfiltered signals.

Filtered electron pulses were fitted with a Gaussian function with almost identical results. A typical example of a 150 GeV electron is shown in Fig. 11a. The signal shape for different electrons is indeed seen to vary very little[2] : the mean value of the FWHM was found to be 4.03 ns with standard deviation 0.09 ns. This may be compared with a standard deviation of 0.20 ns obtained for unfiltered signals. The filtered pion signals are not well described by a Gaussian shape, see Fig. 11b: late tails are present. For the Gaussian component of the filtered pulses from this sample, which contained only pion signals of the type shown in Fig. 5b and 5c, an average FWHM of 6.4 ns was found with a standard deviation of 0.8 ns. The larger values (compared to electromagnetic showers) for both the mean FWHM and its standard deviation reflect the much larger fluctuations in the longitudinal shower development. When the Gaussian component is subtracted, the resulting tail is fit well by an exponential of the form $\exp(-t/T)$, see Fig. 12. The fit gave a mean $T = 9.9$ ns, with a standard deviation of 1.7 ns. This is in good agreement with the value expected[3] for the neutron component that contributes to the hadronic shower signal and thereby to the compensation phenomenon. With this calorimeter technique we can therefore determine the contribution of neutrons to the shower signal on an event-by-event basis. Work on the design of a final matching filter is in progress.

8. Conclusions

We have shown that for the selection of isolated electrons, pion rejection factors similar to those of conventional longitudinally segmented calorimeters can be obtained with the lead and scintillating fiber technique without longitudinal segmentation. The results are obtained using the lateral energy deposit profile, pre-shower detector information, signal timing information, or a combination of these. Pion rejection factors of up to several thousand have been measured in the energy range 40 to 150 GeV. The methods are very simple ones and some of them may be applicable to triggering strategies. It is possible to improve the pion rejection further by using more of the available information, for example the energy distribution between the towers in the numerator of (1) as a means of adjusting the cut on C so that it in effect becomes impact point dependent.

We expect similar rejection factors for other hadrons. As protons and anti-protons have a larger inelastic cross section than pions, the pre-shower detector might be less efficient in rejecting (anti-)protons than pions. As there are many times fewer protons than pions produced this should not pose a problem.

The case of non-isolated electrons has not been addressed in this study. It is the subject of further analysis that is currently underway.

9. Acknowledgements

REFERENCES

1. In this context 'electrons' means 'electrons and positrons'.

2. R. Desalvo *et al*, Nuclear Instruments and Methods **A279**, 467 (1989).

3. D. Acosta *et al*, Nuclear Instruments and Methods **A294**, 193 (1990).

4. Kyowa Gas Chemical Industry Co. LTD, Tokyo, Japan.

5. We define 'nuclear interaction length' in the same way as the Particle Data Group in Physics Letters **B239** (1990), page III5 and 6: it is the mean free path for protons between inelastic interactions. For pions we multiply it by a factor 1.5.

6. R. K. Bock, V. Buzuloiu, W. Krischer, CERN-LAA-RT/90-01 (May 1990).

7. In the calculation the ratio $\sigma(\pi^- p \rightarrow \pi^0 n)/\sigma_{inel}(\pi^- p)$ is needed because λ_I is expressed in terms of σ_{inel}[5], but the measured $\sigma(\pi^- p \rightarrow \pi^0 n)/\sigma_{tot}(\pi^- p)$ is used instead, neglecting the small elastic part of the cross section. To scale from a hydrogen target to a lead or tungsten target one should multiply by $Z/A = 0.40$ to take into account that the charge exchange reaction by negative pions is on protons only. However the charge exchange cross section could scale faster with A then the inelastic cross section, increasing the ratio by a factor two or three. Therefore no scaling factor is applied and a systematic uncertainty of a factor 2 is assigned to the estimates of the charge exchange probabilities. Interactions and conversions are considered in the lead and tungsten parts of the pre-radiator as well as in the S_4 and S_5 scintillation counters, and in the air downstream of S_2 (compare with Sec. 5). The charge exchange cross sections were taken from A.V. Barnes *et al*, Phys. Rev. Lett. **37**, 76 (1976) and the total cross sections from A.S. Carroll *et al*, Phys. Lett. **61B**, 303 (1976).

8. L.P..Caloba, J.M..Seixas and M.N..Souza, SPACAL internal note CERN-LAA-HC/90-013 and -014.

FIGURE CAPTIONS

1. Beam's eye view of the 20 tower calorimeter. Note the numbering of the towers and the points A and B.

2. The beam telescope, beam chambers, and the pre-shower detector positions relative to the calorimeter.

3. The number of events as function of the number of towers that each have an energy exceeding $E_{thr} = 0.4\,\text{GeV}$. Curves are for $80\,\text{GeV}$ electrons (solid line) and pions (dashed line), incident at point A.

4. The containment C for $80\,\text{GeV}$ electrons (a) and pions (b) incident near point A. Note the different horizontal scales.

5. The pulse height in the pre-shower detector (S_6) for $80\,\text{GeV}$ pions (lefthand scale) and electrons (righthand scale). The abscissa is in units of minimum ionizing pulse height.

6. The fraction of pions passing electron selection cuts and the corresponding electron efficiency as function of the containment C. The data are for 80 GeV particles incident at point A.

7. The fraction of pions passing electron selection cuts and the corresponding electron efficiency as function of energy. Also shown is the estimated contribution of the charge exchange reaction. The band indicates the systematic uncertainty.

8. Photomultiplier signals showing the time structure of the calorimeter pulses. In a) several electron signals are overlayed while in b), c), d), and e) individual pion signals are shown. All are for $150\,\text{GeV}$ particles.

9. The distribution of Full Width at one Fifth Maximum (FWFM) for $80\,\text{GeV}$ electrons and pions. Data from impact points A and B are plotted together.

10. The fraction of pions that pass the electron selection cuts and the corresponding electron efficiency as function of the cut on the FWFM. The data are for $80\,\text{GeV}$ particles, impact points A and B are plotted together.

11. An example of a digitized filtered $150\,\text{GeV}$ electron signal (a) and pion signal (b). The bin size is $1\,\text{ns}$ and the $t = 0$ point is arbitrary. The Gaussian fits are described in the text.

12. An example of a digitized filtered $150\,\text{GeV}$ pion signal after subtraction of the Gaussian component. The bin size is $1\,\text{ns}$ and the $t = 0$ point is arbitrary.

TABLE CAPTIONS

1. Fraction of pions passing electron selection cuts and electron efficiencies obtained by counting the number of towers over the indicated energy thresholds. A cut at 7 towers is used, see text.

2. Fraction of pions passing electron selection cuts and electron efficiencies obtained with a containment cut $C \geq 0.970$.

3. Fraction of pions passing electron selection cuts and electron efficiencies obtained with a 1.75 minI cut on the pre-shower detector pulse height.

4. Fraction of pions passing electron selection cuts, correlation coefficients, electron efficiencies, and the contribution from charge exchange for combined cuts on containment and pre-shower detector pulse height.

5. Fraction of pions passing electron selection cuts and electron efficiencies obtained with a timing cut.

Table 1				
E (GeV)	E_{thr} (MeV)	point	π-pass (%)	e-eff (%)
40	200	A	1.35 ± 0.34	98.2 ± 0.5
80	400	A	1.00 ± 0.29	98.8 ± 0.3
150	600	A	0.26 ± 0.13	98.1 ± 0.4
40	200	B	2.55 ± 0.47	99.7 ± 0.2
80	300	B	0.49 ± 0.20	98.4 ± 0.4
150	500	B	0.50 ± 0.18	98.4 ± 0.4

Table 2			
E (GeV)	point	π-pass (%)	e-eff (%)
40	A	1.90 ± 0.49	95.8 ± 0.6
80	A	0.65 ± 0.17	98.8 ± 0.3
150	A	0.55 ± 0.16	99.3 ± 0.3
40	B	1.91 ± 0.40	95.3 ± 0.7
80	B	0.39 ± 0.17	99.1 ± 0.3
150	B	0.93 ± 0.24	99.5 ± 0.2

Table 3		
E (GeV)	π-pass (%)	e-eff (%)
40	7.8 ± 0.7	96.9 ± 0.4
80	7.4 ± 0.6	97.8 ± 0.3
150	8.2 ± 0.7	99.2 ± 0.2

Table 4					
E (GeV)	point	π-pass (%)	corr	e-eff (%)	ch-exch (%)
40	A	$(6.4 \pm 0.8) \times 10^{-2}$	-0.81	95.2	2×10^{-3}
80	A	$(3.5 \pm 0.6) \times 10^{-2}$	-0.32	96.3	8×10^{-4}
150	A	$(4.6 \pm 0.7) \times 10^{-2}$	0.02	99.0	4×10^{-4}
150	B	$(4.2 \pm 0.7) \times 10^{-2}$	-0.60	99.0	4×10^{-4}

Table 5		
E (GeV)	π-pass (%)	e-eff (%)
40	1.6 ± 0.3	100.00
80	0.12 ± 0.08	99.69
150	0.28 ± 0.12	99.94
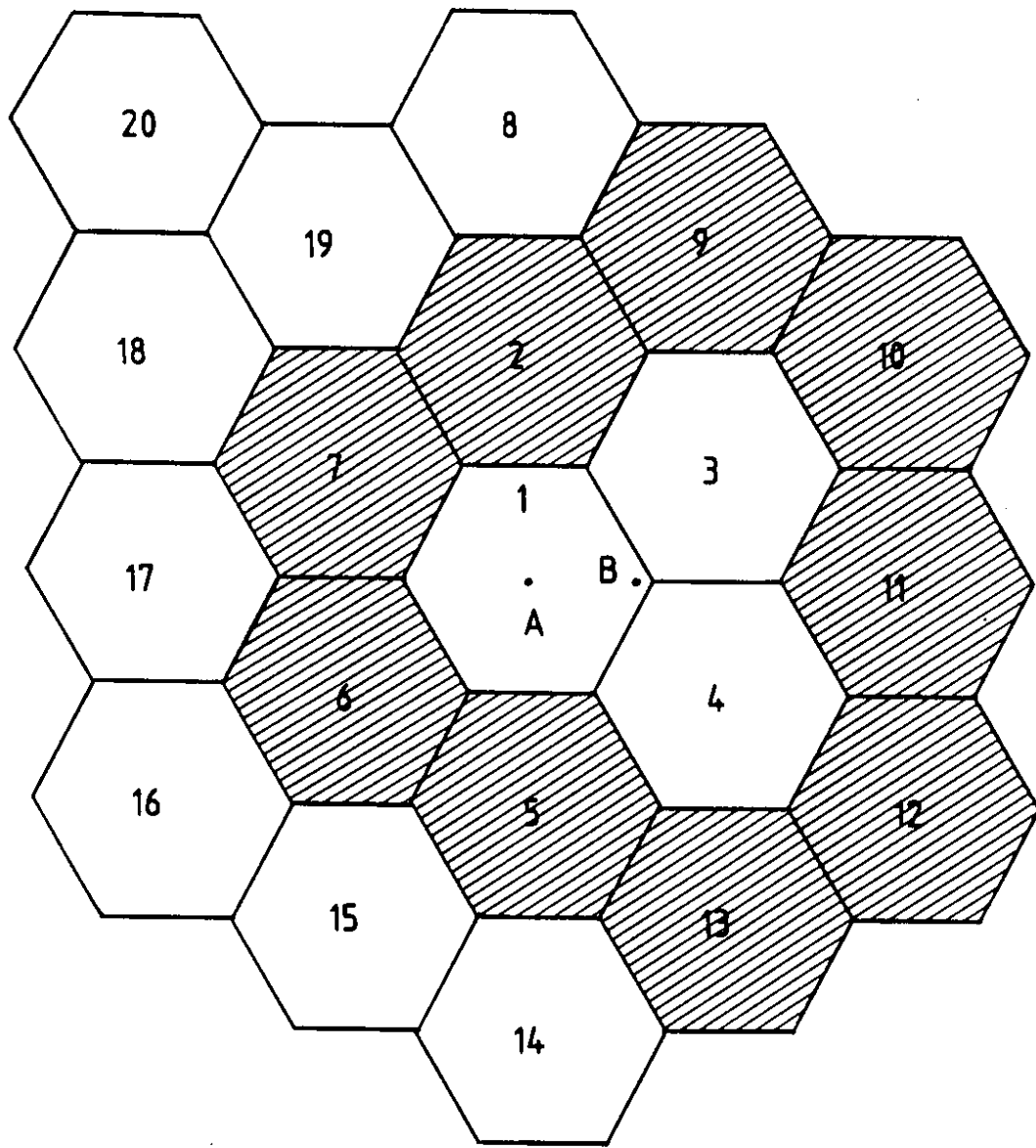
Figure 1

BEAM ELEMENTS
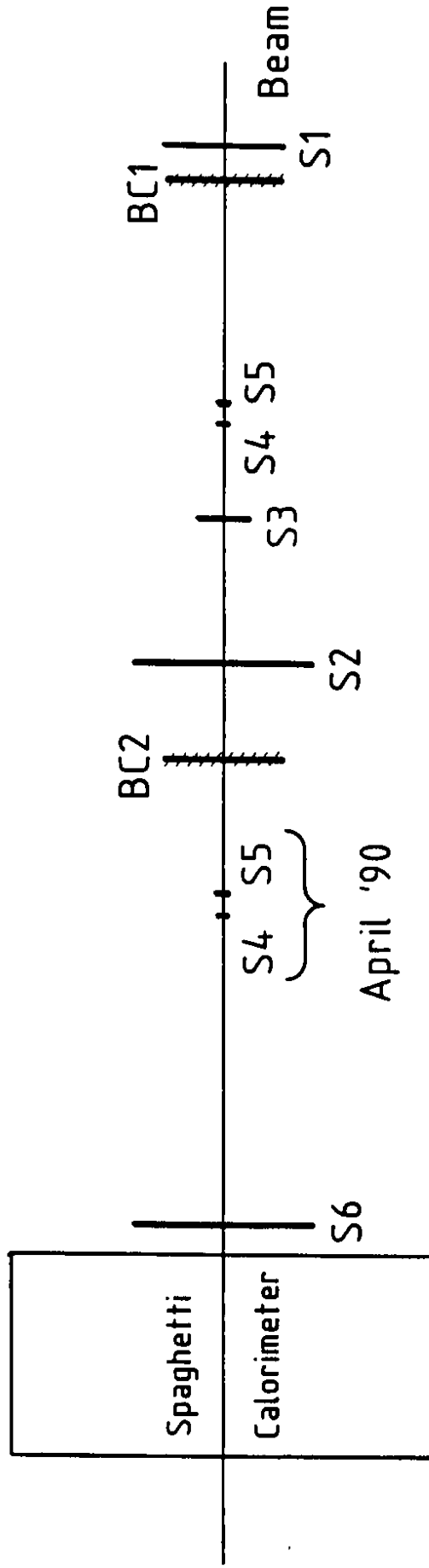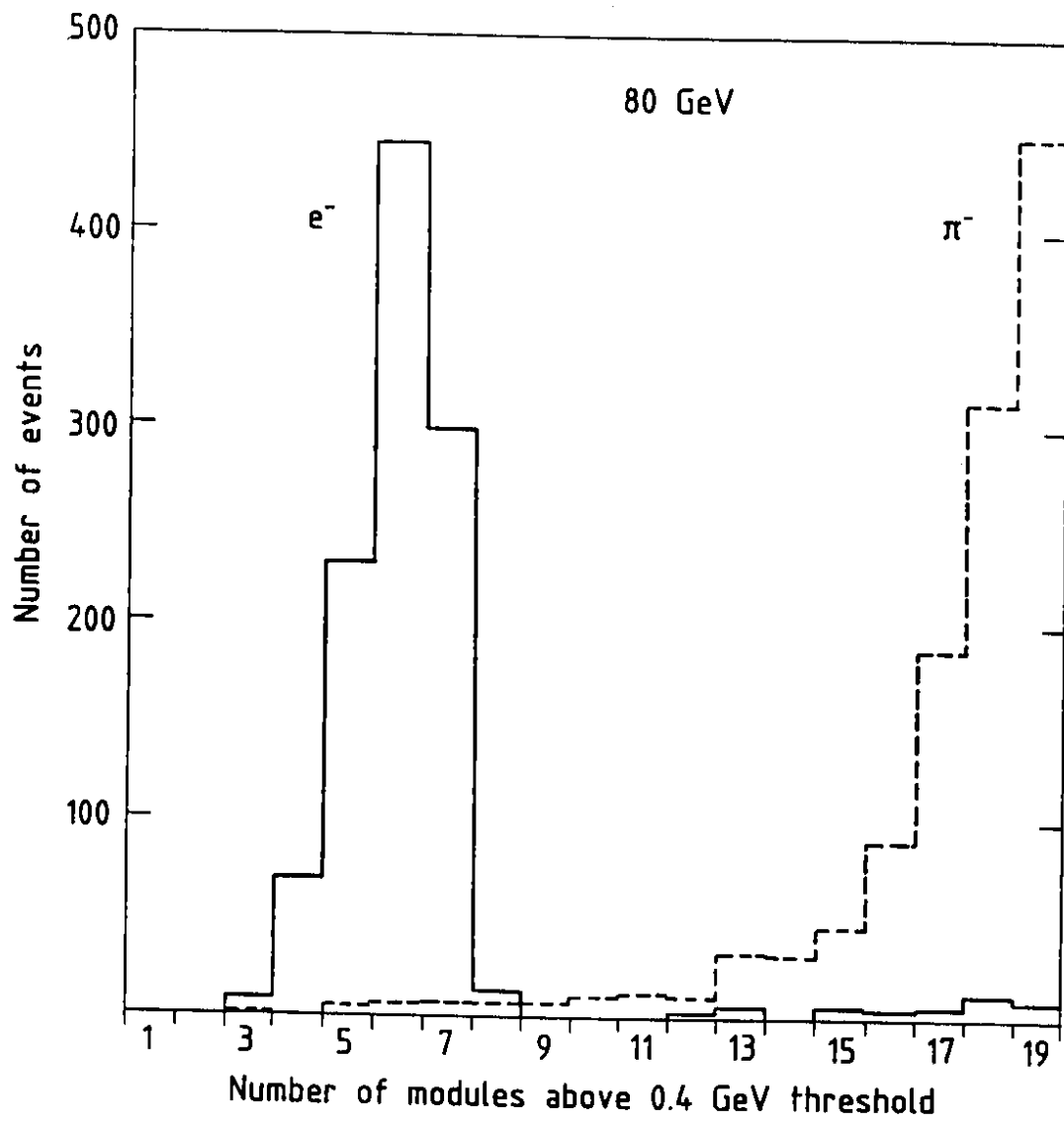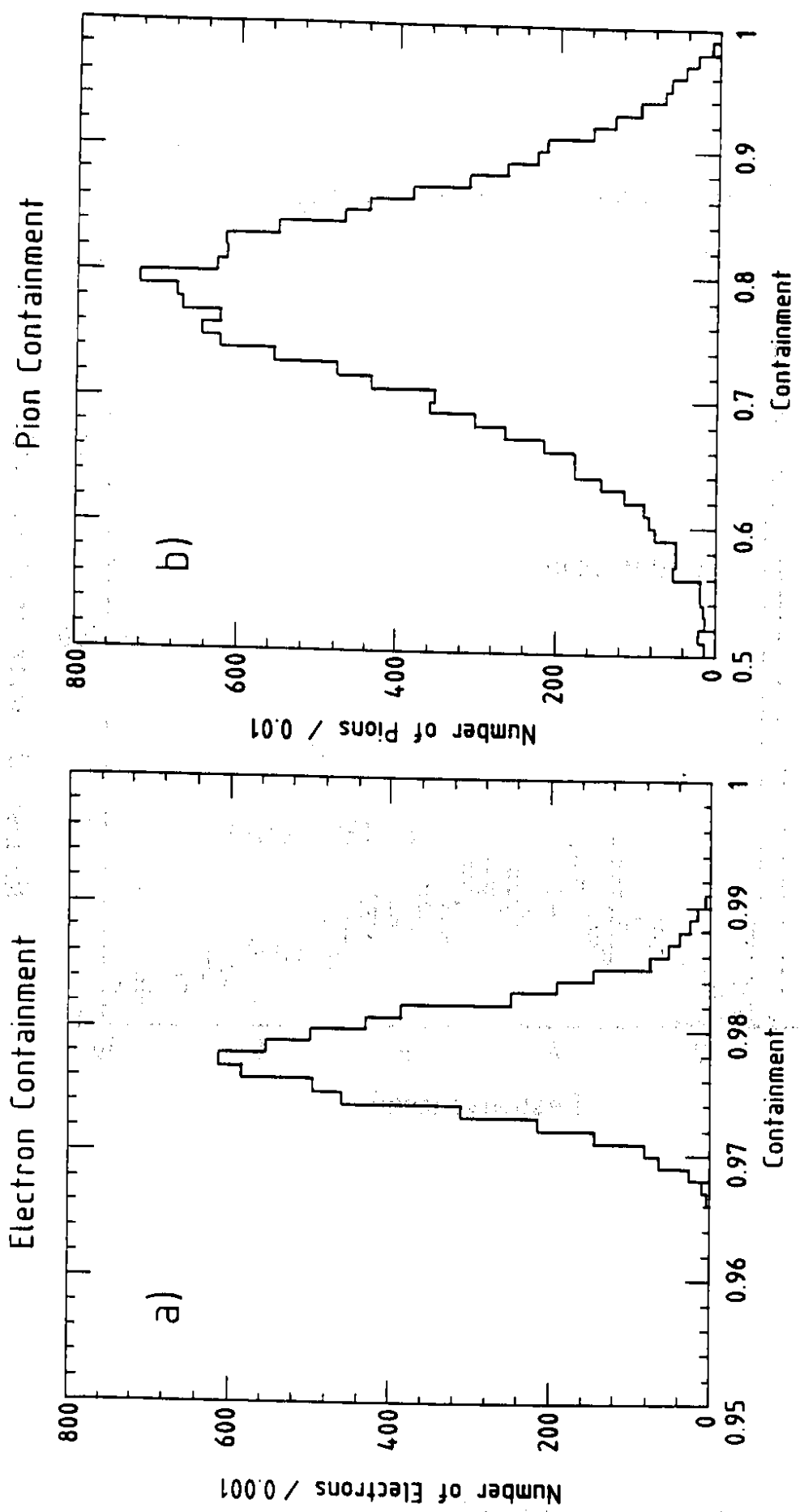
Figure 2

Figure 3

Figure 4

Pre-Shower Detector Response

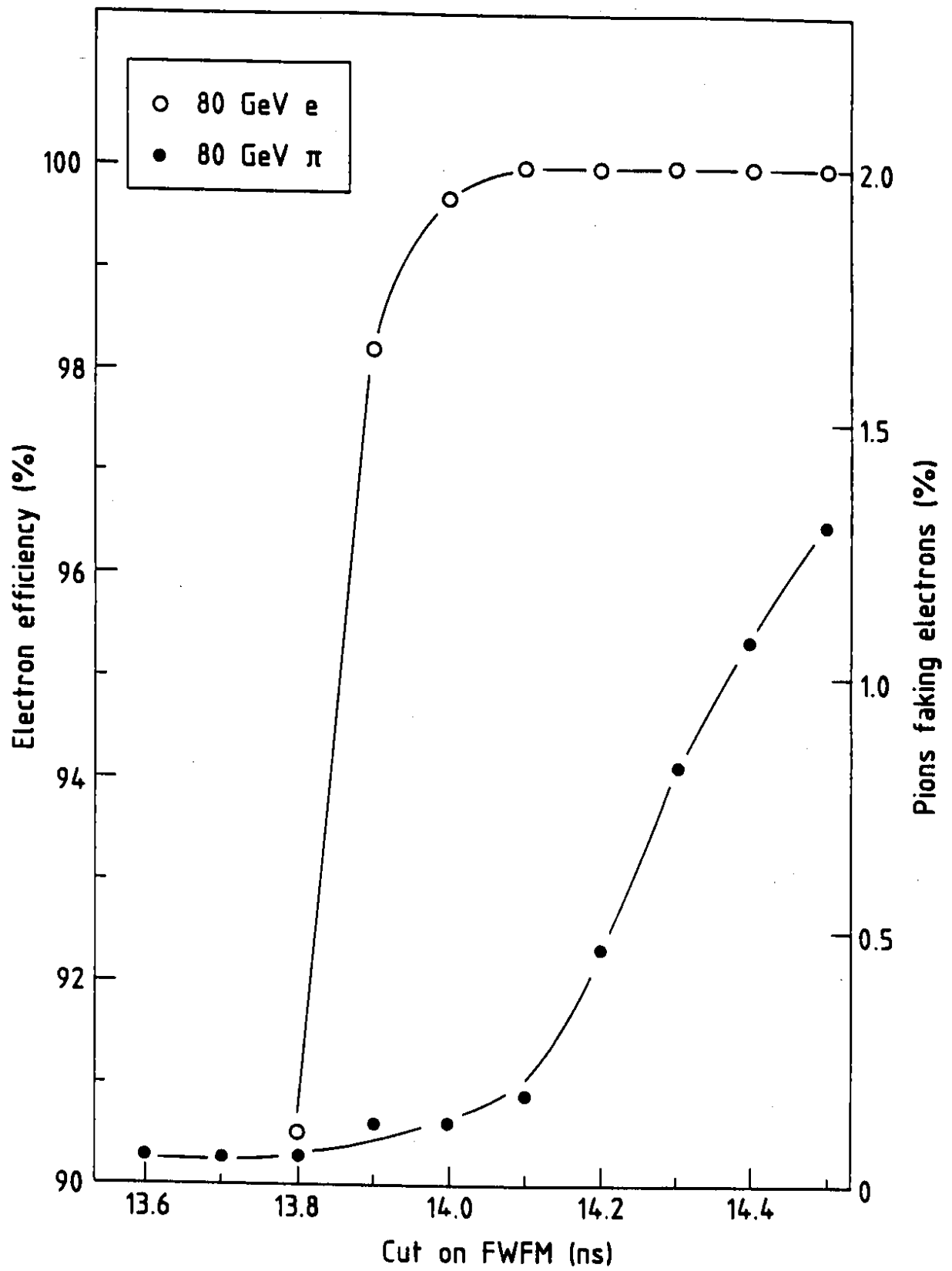
π⁻ (LH scale)

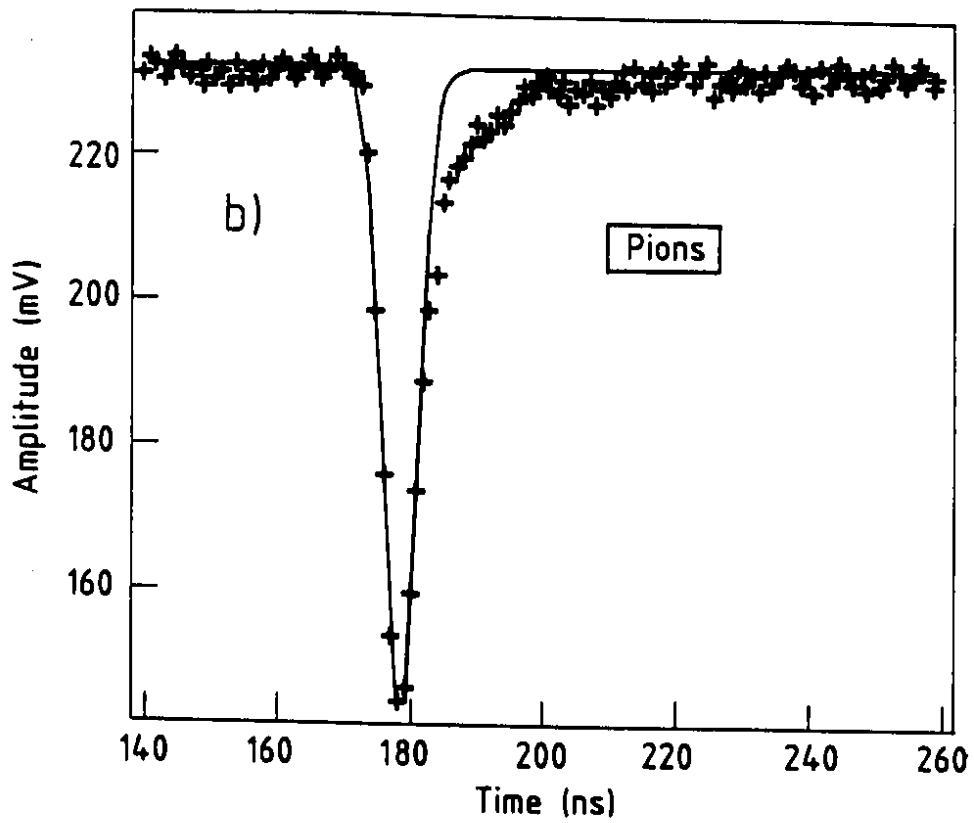e⁻ (RH scale)
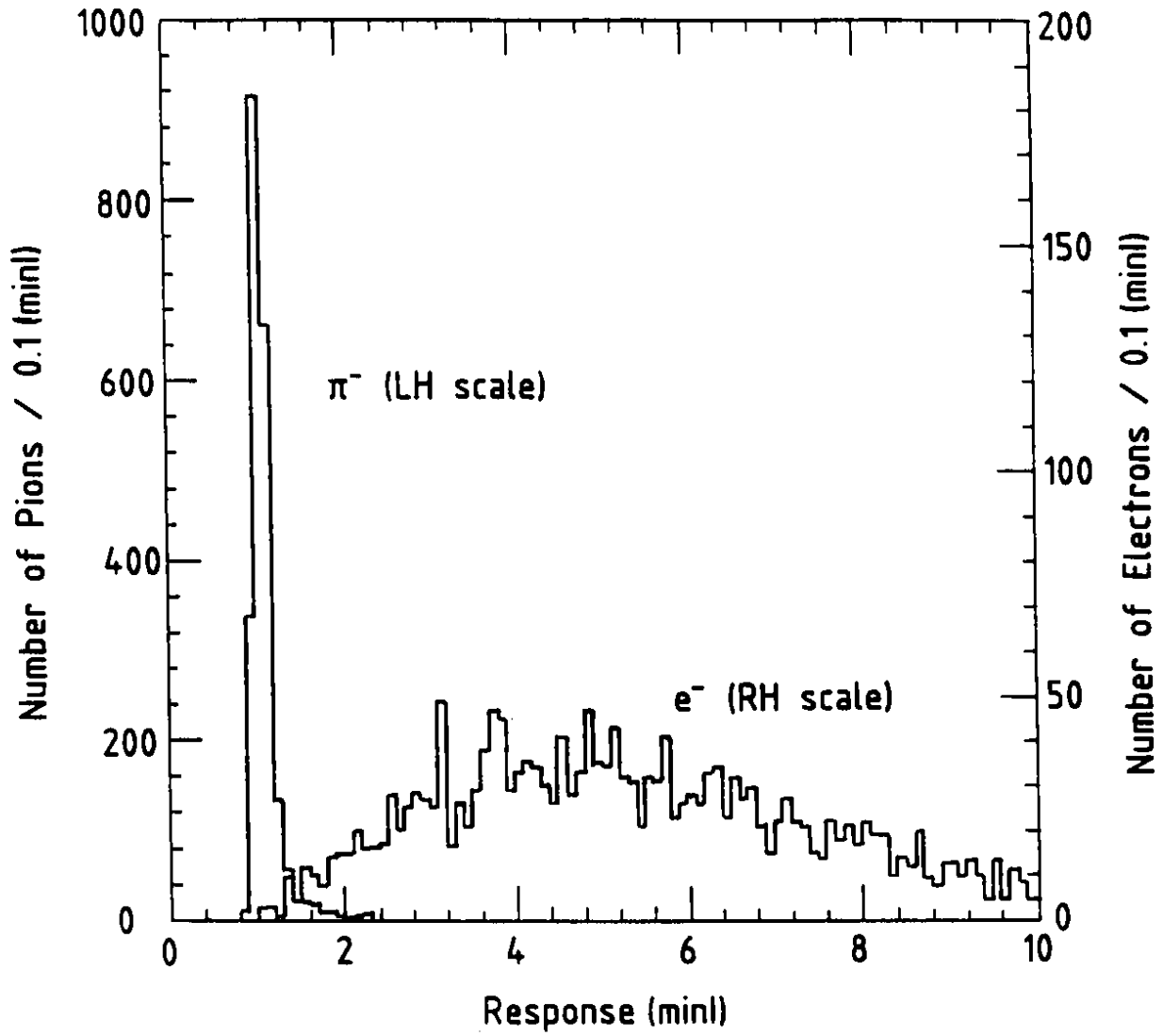
Figure 5

e/π Separation at 80 GeV
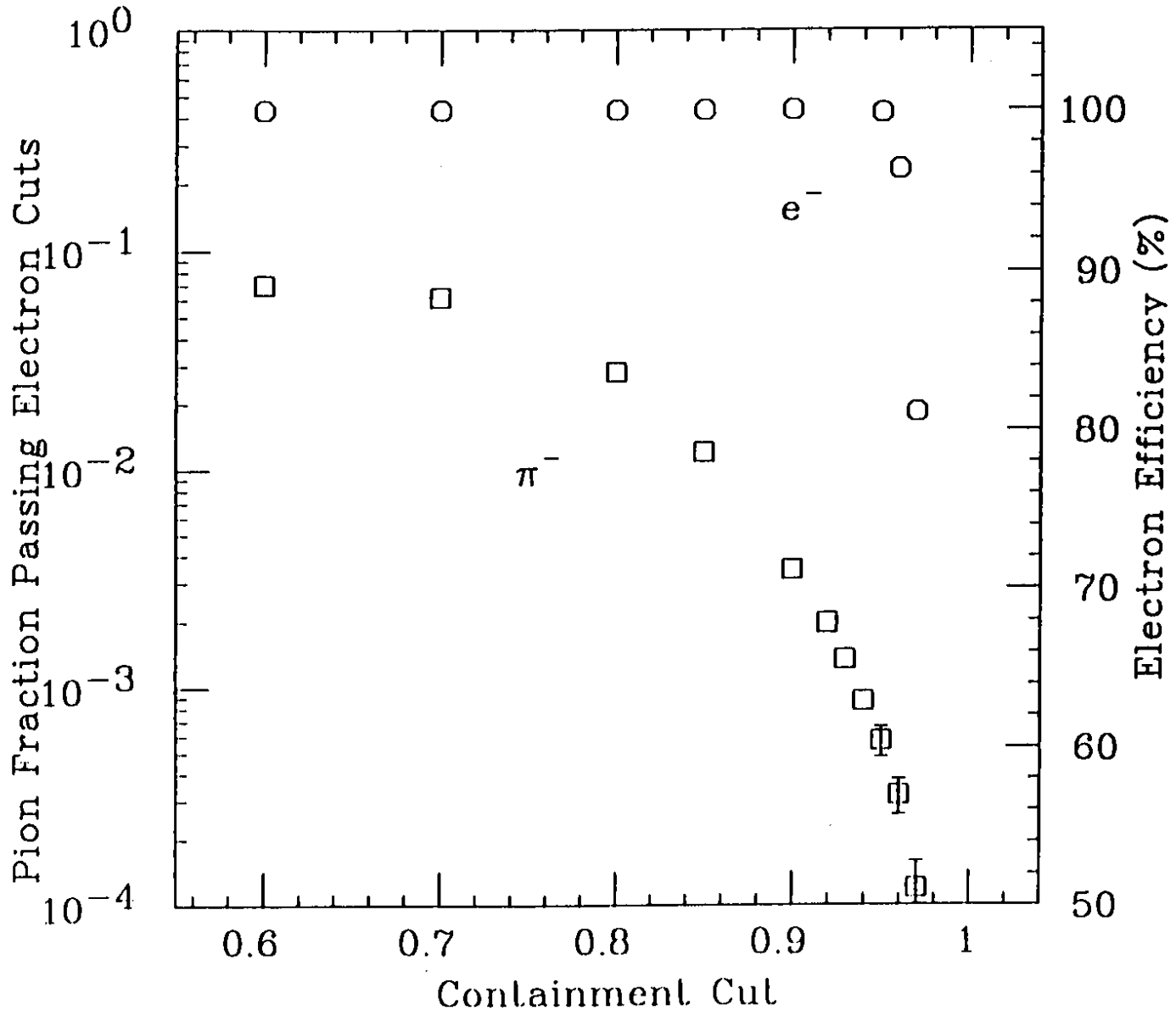
Figure 6
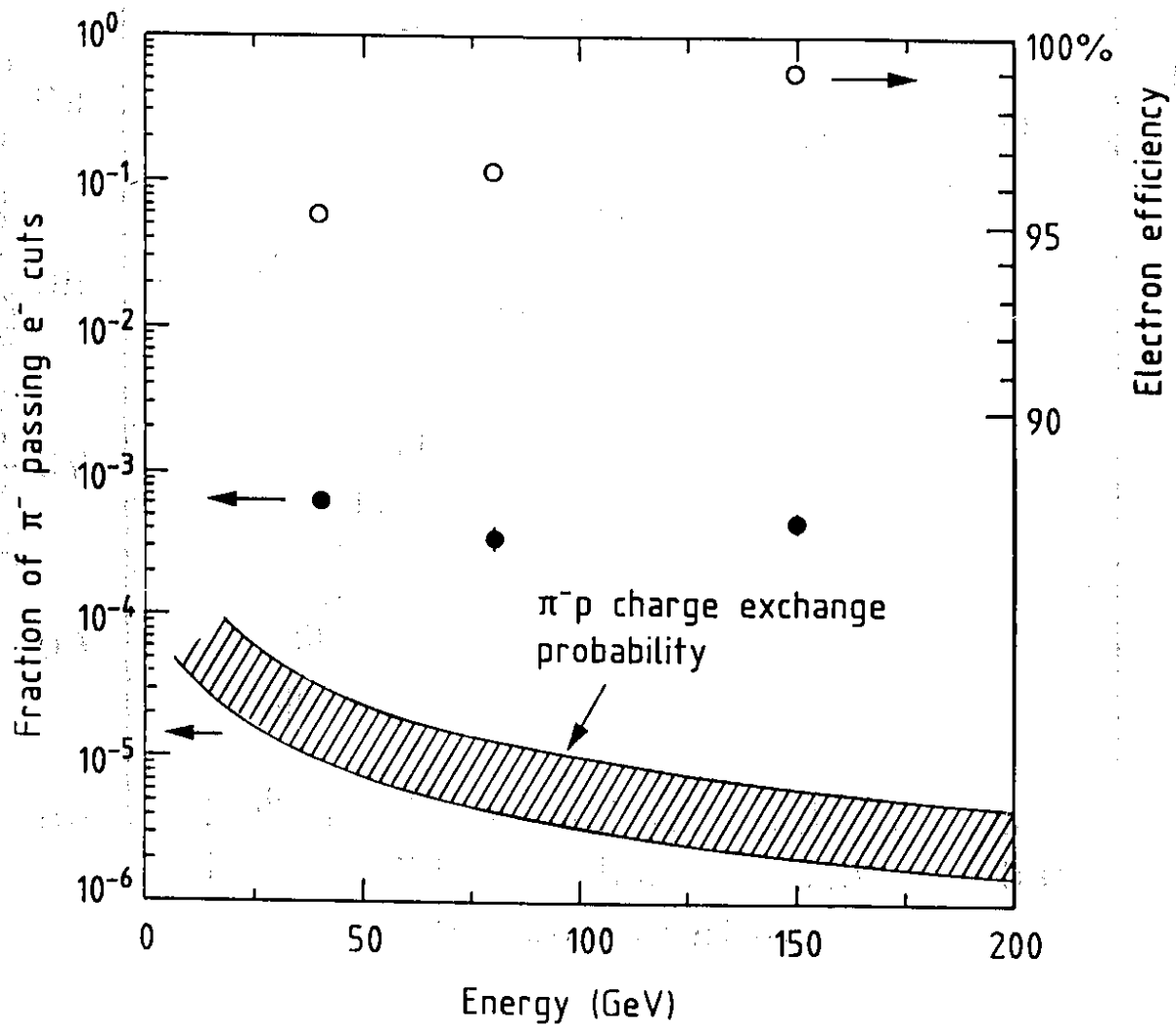
Figure 7
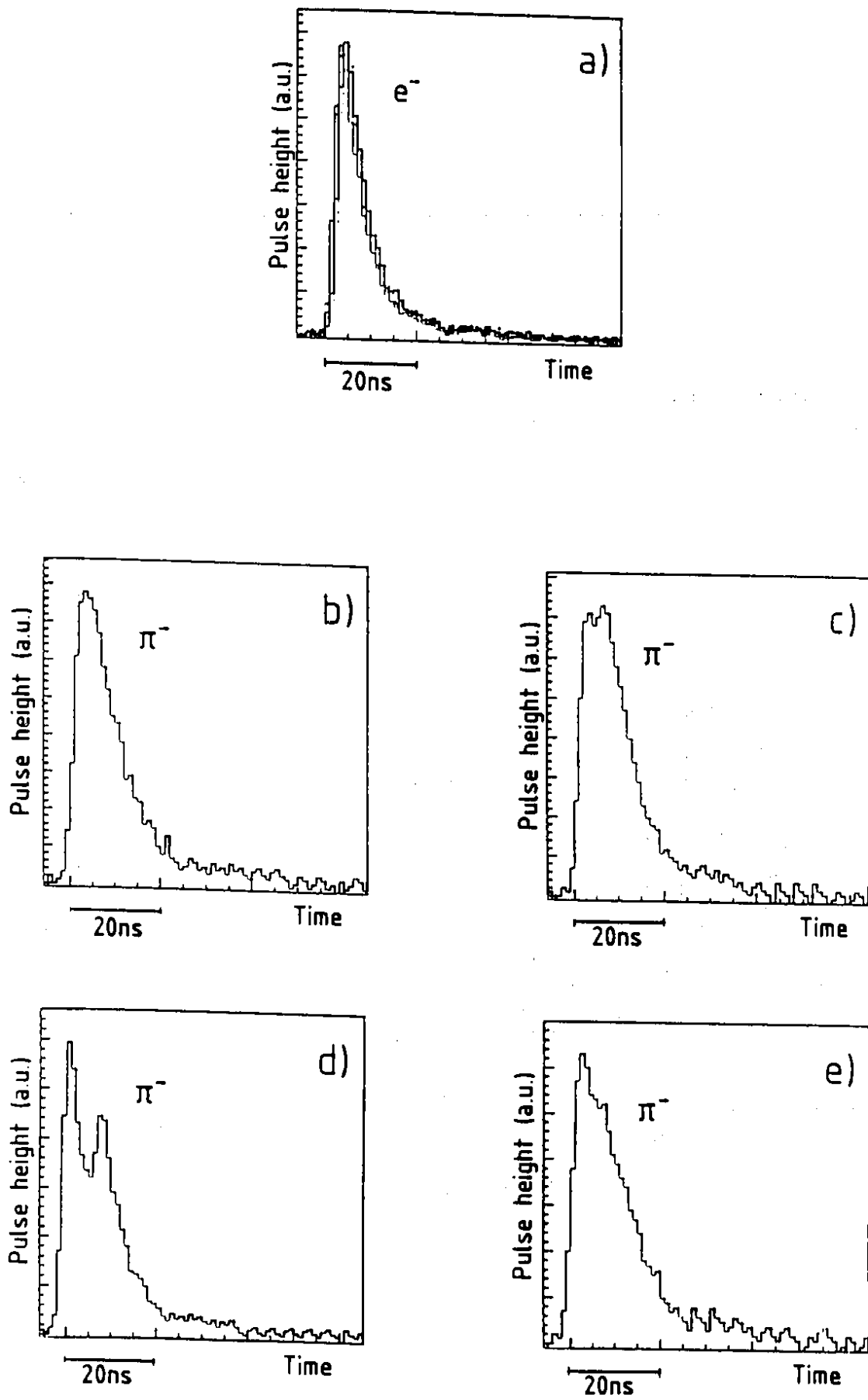
Figure 8
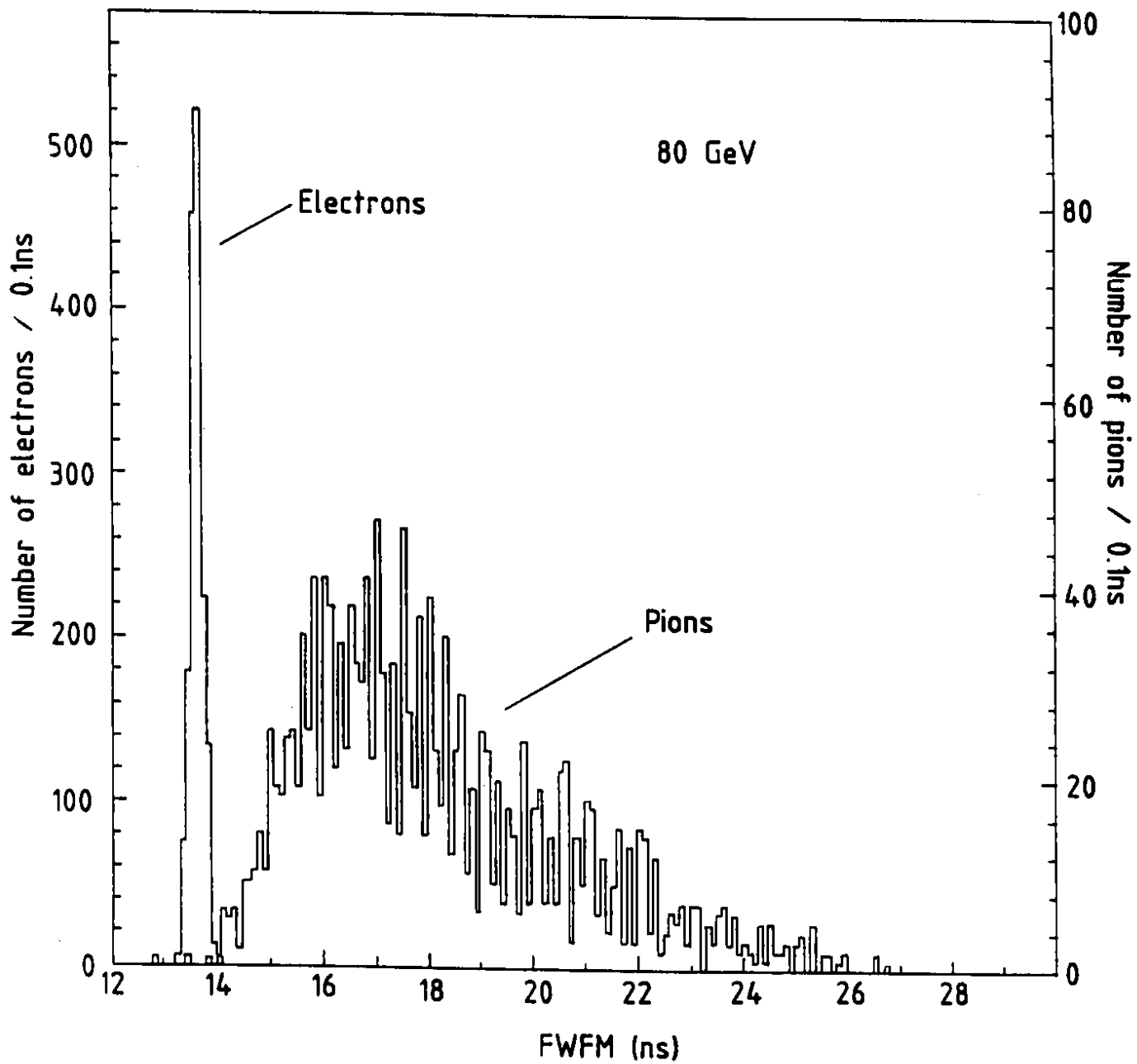
Figure 9

Figure 10

Figure 11

Figure 12